Catalysis Today 174 (2011) 106–113

Contents lists available at ScienceDirect

Catalysis Today

journal homepage: www.elsevier.com/locate/cattod

Synthesis of mesoporous Nb_2O_5 photocatalysts with Pt, Au, Cu and NiO cocatalyst for water splitting

Hsin-Yu Lin [a,*], Hsien-Chang Yang [b], Wei-Lin Wang [a]

[a] Department of Materials Science and Engineering, National Dong Hwa University, Hualien, Taiwan
[b] Energy and Environment Research Laboratories, Industrial Technology Research Institute, Hsinchu, Taiwan

ARTICLE INFO

Article history:
Received 14 October 2010
Received in revised form 4 January 2011
Accepted 25 January 2011
Available online 21 March 2011

Keywords:
Niobium oxide
Mesoporous
Water splitting
Photocatalyst
Hydrogen production

ABSTRACT

Hydrogen production by water splitting was examined over mesoporous niobium oxide photocatalysts, prepared by evaporation-induced self-assembly (EISA) method. A series of Pt, Au, Cu and NiO nanoparticles were loaded as cocatalyst to enhance the photocatalytic activity of mesoporous niobium oxide. The influences of the preparation parameters on the characteristics of the mesoporous niobium oxide photocatalysts and their photocatalytic activities were investigated in detail. The catalysts were characterized by powder X-ray diffraction (XRD), Transmission Electron Microscopy (TEM), N_2 sorption and ultraviolet–visible spectroscopy (UV–vis) and nitrogen adsorption–desorption isotherm. The photocatalytic water splitting are preformed in an aqueous MeOH, used as sacrificial hole scavengers under UV light irradiation. The rate of H_2 evolution from an aqueous methanol solution under UV irradiation significantly changed with the variation of loading metal, and Pt loaded niobium oxide catalyst exhibited the highest photoactivity, with a rate of H_2 production of 4647 μmol h^{-1} g^{-1} which was about 2.2, 2.9 and 6.5 times than Au, Cu and NiO photocatalysts, respectively.

1. Introduction

To overcome environmental problems related to green house gas emissions and to fulfill the energy needs of future generations, much research efforts have been devoted to developing sustainable and renewable energy sources, which are environmental friendly. There has been much interest in finding ways to produce hydrogen gas from renewable energy sources such as solar and wind to avoid the emission of greenhouse gases inevitably released by its production from fossil fuels. In 1972, Fujishima and Honda [1] first reported the use of semiconductor catalysts for splitting water with ultraviolet radiation. Since then, photocatalysis has attracted much attention and the conversion of solar energy into clean hydrogen energy has been widely investigated. Transition metal oxides with d^0 electron configuration, such as $SrTiO_3$ [2], $Rb_2La_2Ti_3O_{10}$ [3], and $Sr_2Nb_2O_7$ [4], and p-block metal oxides with d^{10} electron configuration, such as $M_2Sb_2O_7$ (M = Ca, Sr) [5], and $In(OH)_ySz$:Zn [6], have been reported to be active in splitting water into its components H_2 and O_2. Furthermore, photocatalytic activity can be improved by loading metal particles (Pt in most cases [7–9]) and metal oxide particles (such as NiO [10,11], RuO_2 [7]) as cocatalysts. These cocatalysts can change the distribution of electrons and can prevent effectively electron–hole recombinations, thereby enhancing photocatalytic efficiency.

In general, solid-state reaction is widely employed to synthesize semiconductor photocatalyst. However, the high-temperature synthesis process yields large particles and low surface area. Therefore, synthesis of mesoporous transition metal oxides offers a chance for developing high-performance photocatalysts because of their high surface area. In our previous work [12], we studied synthesis of a series mesoporous In-Nb mixed oxides and their photocatalytic properties. The mesoporous Nb_2O_5 synthesized by triblock copolymer as a template and exhibited high photocatalytic activity for water-splitting reaction. In addition, In-Nb-mixed oxides were found to show high photocatalytic reactivity in producing hydrogen, and its reactivity was much higher than powdered TiO_2 (P-25) catalysts. A drawback of this approach is the apparent difficulty to increase the incorporation of indium cations in the framework of mesoporous Nb_2O_5.

In this paper, we present the synthesis of a series of novel mesoporous Nb_2O_5 with noble metal (Pt, Au) and base metal/metal oxide (Cu and NiO) cocatalyst. The mesoporous Nb_2O_5 with Pt and Au cocatalyst was prepared by photodeposition method. On the other hand, the mesoporous Nb_2O_5 with Cu cocatalsyt was prepared by impregnation method followed by reduction procedure, where the heat-treatment temperature was up to 500 °C. Hence, this work is also carried out to understand the influence of calcination temperature on the properties of mesoporous Nb_2O_5. The catalysts were studied using powder X-ray diffraction (XRD), transmission

* Corresponding author. Tel.: +88 638634231.
E-mail address: hsinyu@mail.ndhu.edu.tw (H.-Y. Lin).

0920-5861/$ – see front matter © 2011 Elsevier B.V. All rights reserved.
doi:10.1016/j.cattod.2011.01.052

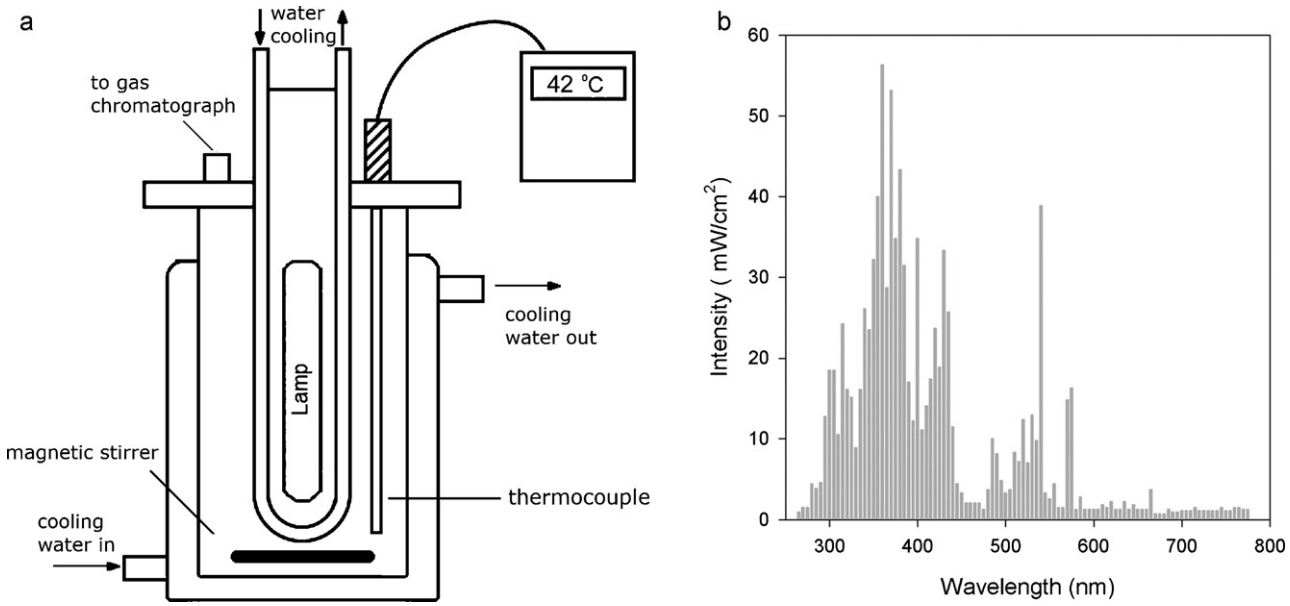

Fig. 1. (a) Closed reaction system for photocatalysis water splitting and (b) emission spectrum of 400 W medium-pressure metal halide lamp (λ_{max} = 360 nm, UV irradiation 150 mW/cm^2).

electron microscopy (TEM), nitrogen sorption measurement, and ultraviolet–visible spectroscopy (UV–vis). Photocatalytic water-splitting is preformed in an aqueous MeOH, used as sacrificial scavengers under UV light irradiation.

As we show in this paper, significant enhancing effects from the loading of metal nanoparticles as cocatalyst on mesoporous niobium oxide were observed in the hydrogen production of photocatalytic water splitting reaction. The Pt/meso-Nb_2O_5 catalyst showed a uniform dispersion of Pt nanoparticles with an average Pt particle size of 2 nm and exhibited the highest photocatalytic water splitting activity (4647 μmol h^{-1} g^{-1}), which was about 10 times higher than that exhibited by meso-Nb_2O_5 catalyst.

2. Experimental

The mesoporous Nb_2O_5 photocatalyst was prepared by an evaporation-induced self-assembly (EISA) method, as reported by Yang et al. [13]. In a typical preparation, 2.0 g of P123 (Sigma-Aldrich) was dissolved in anhydrous ethanol (Sigma-Aldrich), followed by addition of 0.01 mol $NbCl_5$ (Alfa Aesar) under stirring for 40 min. Then, 0.2 g of deionized water was added to the solution. The solution was mixed under vigorous stirring for 5 days at 40 °C and the gel was then obtained. Subsequently, the gel was first calcined at 450 °C for 5 h for removing the template and then calcined again at 450 °C, 500 °C, and 650 °C for 1 h, designated as m450-Nb_2O_5, m500-Nb_2O_5, and m650-Nb_2O_5, respectively, to crystallize the framework while maintaining the mesoporous structure [14,15].

The mesoporous Nb_2O_5 photocatalyst with Au and Pt cocatalyst were synthesized by photodeposition method. First, 1.0 g of m450-Nb_2O_5 was dispersed into 550 cm^3 of deionized water. Then the required amount of aqueous solution of $HAuCl_4{\cdot}3H_2O$ or $H_2PtCl_6{\cdot}6H_2O$ (1 wt% Au or Pt loading for a complete photoreduction) was added to the solution with thorough stirring at 60 °C. The suspension was irradiated in a photoreactor with a 400 W medium-pressure metal halide lamp (Phillips HPA400) for 3 h under string at 60 °C. The precipitates were filtered and washed carefully until all chlorine ions were removed. Then, the samples were dried at 80 °C overnight. The samples were denoted as Pt/m-Nb_2O_5 and Au/m-Nb_2O_5.

The mesoporous Nb_2O_5 photocatalyst with Cu and NiO (1 wt%) cocatalyst were prepared by incipient wetness impregnation. The required amount of aqueous solution of $CuCl_2{\cdot}2H_2O$ (J.T. Baker) or $Ni(NO_3)_2{\cdot}6H_2O$ (J.T. Baker) was slowly added to m450-Nb_2O_5. Following the impregnation process, the sample was dried at 60 °C overnight. Then, the NiO/m450-Nb_2O_5 samples were calcined at 350 °C. Furthermore, the Cu/m450-Nb_2O_5 samples were calcined at 500 °C in air for 2 h and reduced in a H_2/Ar (5/95) stream at 300 °C for 3 h under a heating rate of 10 K/min.

The characterization methods included powdered X-ray diffraction (XRD, Rigaku X-ray diffractometer MAX-2500 V, Cu Ka radiation, λ = 1.54178 Å), UV–vis diffuse reflectance spectra were measured (Varian Lary 5E diode array spectrometer) and transmission electron microscopy (TEM, JEOL JEM-2000FX microscope). The N_2 adsorption–desorption isotherms were measured at −196 °C on a Qantachorme, Autosorb-1-C sorptometer. The surface areas were calculated by BET equation and the BJH pore size distributions were calculated from the desorption isotherms.

The photocatalytic reaction was carried out in a reactor equipped with an inner irradiation quartz cell with a cooling water jacket as shown in Fig. 1. A 400 W medium pressure halide lamp (Phillips HPA400, λ_{max} = 360 nm, irradiation 150 mW/cm^2) was mounted inside the quartz cell. The photocatalytic H_2 evolution of water splitting was performed in 550 ml aqueous methanol solution (vol. ratio of MeOH: H_2O = 1:5) containing about 0.2 g catalyst at 43 °C. The gas product was analyzed by a gas chromatography (China Gas Chromatography 9800) with a packed column (MS-5A, 3.5 m in length) and thermal conductivity detector.

3. Results and discussion

3.1. Characterization of the mesoporous Nb_2O_5 and cocatalyst loaded mesoporous Nb_2O_5 catalysts

The XRD patterns of mesoporous Nb_2O_5 obtained using different thermal treatment conditions were shown in Fig. 2. As can be seen, m450-Nb_2O_5 showed a large and broad the peak at about 2θ = 25° and the absence of any crystallite peaks of Nb_2O_5 indicated the catalysts were amorphous or the corresponding Nb_2O_5 crystallite sizes in the catalysts were too small to be detected by

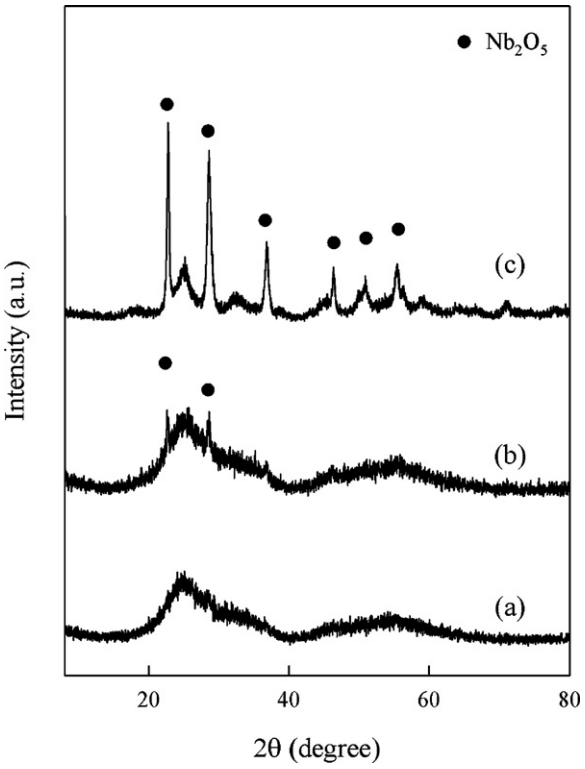

Fig. 2. XRD patterns of (a) m450-Nb_2O_5, (b) m500-Nb_2O_5 and (c) m650-Nb_2O_5.

the instrument. Small reflection peaks of Nb_2O_5 were detected at $2\theta = 22.6^\circ$ and 28.3° (Nb_2O_5 (0 0 1 and (180)) diffraction line, JCPDS #30-0873) in XRD pattern of m500-Nb_2O_5 catalyst. The intensity of characteristic peaks of Nb_2O_5 in XRD pattern was increased with increasing calcination temperature, indicating the

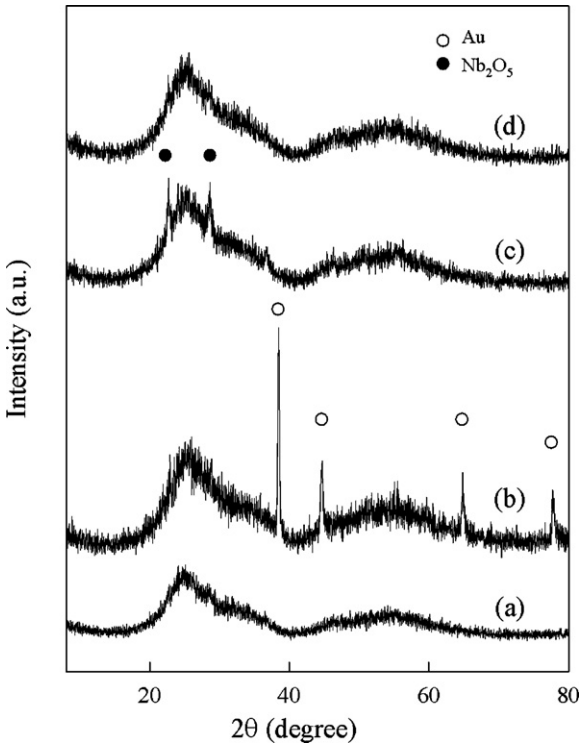

Fig. 3. XRD patterns of (a) Pt/m-Nb_2O_5, (b) Au/m-Nb_2O_5, (c) Cu/m-Nb_2O_5 and (d) NiO/m-Nb_2O_5.

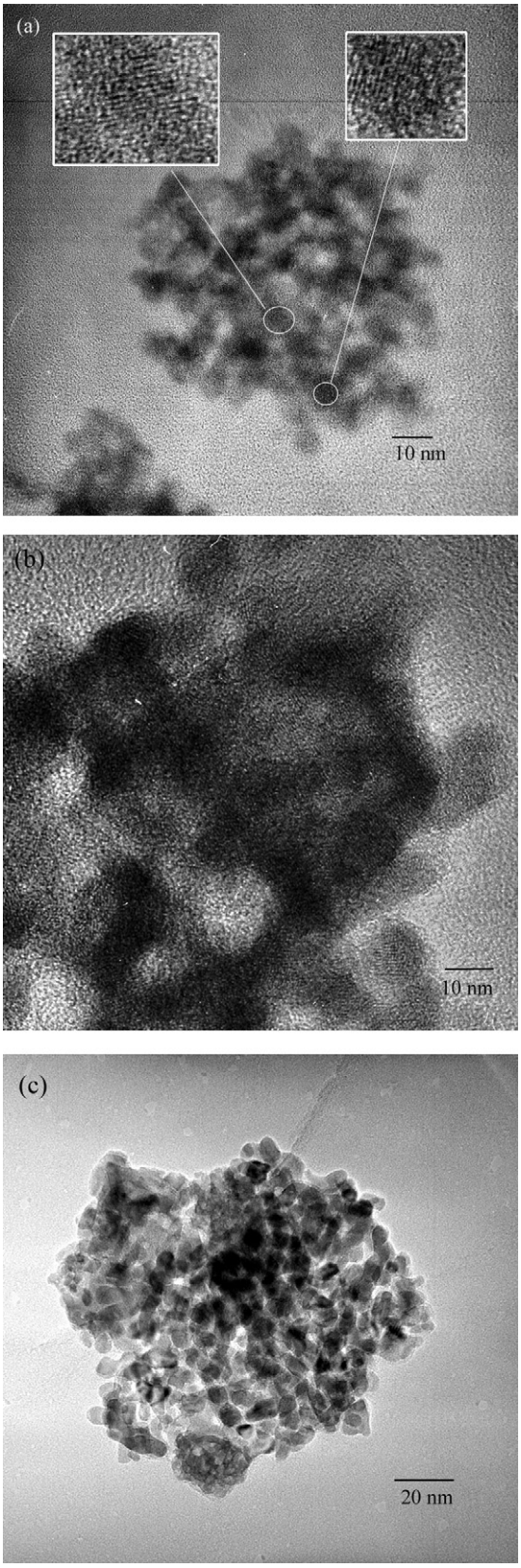

Fig. 4. TEM images of (a) m450-Nb_2O_5, (b) m500-Nb_2O_5 and (c) m650-Nb_2O_5.

Nb_2O_5 crystallite size was increased with the calcination temperature increasing. The crystallite sizes of m650-Nb_2O_5 was about 30 nm determined by Nb_2O_5 (0 0 1) peak according to the Scherrer formula.

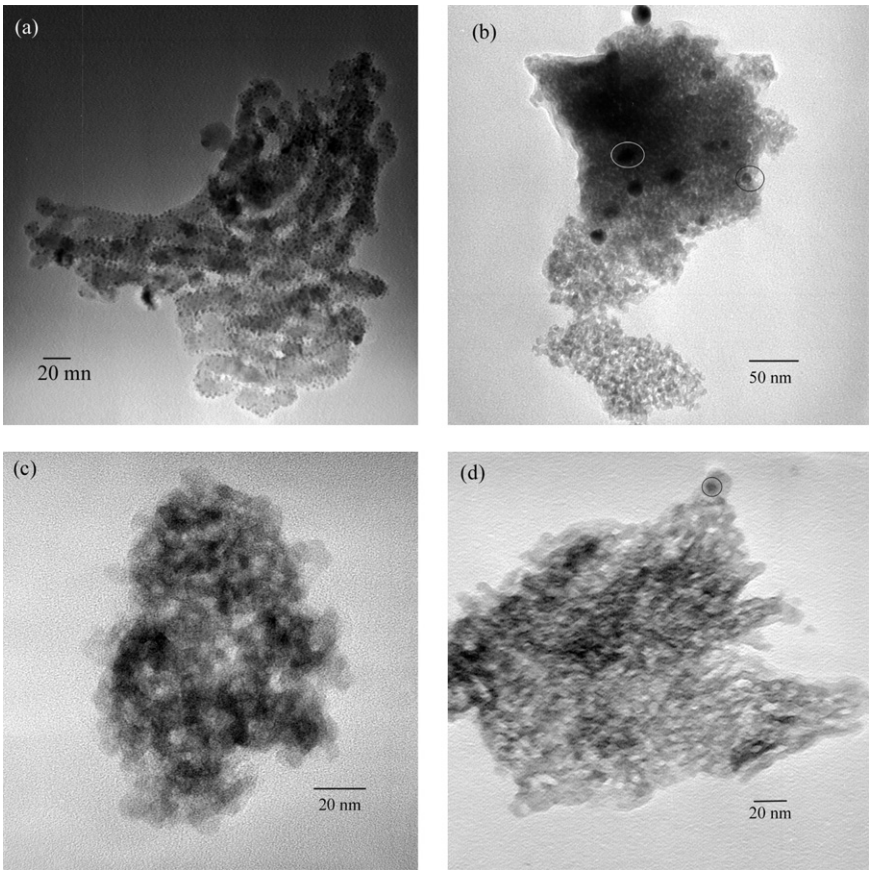

Fig. 5. TEM images of (a) Pt/m-Nb_2O_5, (b) Au/m-Nb_2O_5, (c) Cu/m-Nb_2O_5 and (d) NiO/m-Nb_2O_5.

Fig. 3 shows the XRD patterns of the Au, Pt, Cu and NiO-loaded m450-Nb_2O_5 catalysts, which were obtained with m450-Nb_2O_5 as the reference material (Fig. 2(a)). As seen in Fig. 3(b), the Pt/m-Nb_2O_5 show no diffraction peaks either of metallic platinum or of platinum oxide. It reveals that particles of platinum species on the m450-Nb_2O_5 surface are amorphous or very small and highly dispersed within the matrix. On the other hand, the photodeposition method was also used to prepare the Au/m-Nb_2O_5 sample, whose XRD pattern was shown in Fig. 2(b). As can be seen, the diffraction signals of gold in the spectra become more visible. The Au (1 1 1) diffraction line is positioned at $2\theta = 38.28^\circ$, and other characteristic XRD peaks for gold, particularly at $2\theta = 44.48^\circ$ (Au (2 0 0)) and 64.58° (Au (2 2 0)) were also observed in the spectra which are related to metallic gold and no peaks of Au_2O or Au_2O_3 are observed. According to the peaks and Scherrer formula, the diameter of crystalline particles of gold was calculated to be 35.6 nm with 2θ of 38.28°. The difference of Pt and Au particle size on mesoporous Nb_2O_5 surface was further evident by TEM (see Fig. 5 (a) and (b)).

The XRD patterns of Cu and NiO loaded m-Nb_2O_5 prepared by incipient wetness impregnation are shown in Fig. 3(c) and (d), respectively. As seen in Fig. 3(c), only the peaks of niobium oxide are observed but no peaks of Cu-related compounds are detected. The Cu/m-Nb_2O_5 sample was prepared by the incipient wetness impregnation method, and then calcined in air at 500 °C. It can be deduced that the tendency of high calcination temperature towards a slight increase in crystal size of Nb_2O_5 is still evident. Fig. 3(d) shows that the NiO/m-Nb_2O_5 sample after calcination at 350 °C has no diffraction peaks of niobium oxide either, implying fairly good dispersion of Ni species over the m-Nb_2O_5 surface.

To obtain information on their size and morphology, the catalysts were subjected to transmission electron microscopy (TEM) analysis. Fig. 4 depicts the TEM images of m450-Nb_2O_5, m500-Nb$_2O_5$ and m650-Nb_2O_5 catalysts. As seen in Fig. 4, the m450-Nb_2O_5 sample displayed the patterns characteristic of the mesoporous structure with a wormhole channel fashion [14]. It should be noticed that the framework of m450-Nb_2O_5 were consisted with ultra fine Nb_2O_5 crystallites (see inset of Fig. 4(a)). It can also be observed that the sample calcined at 650 °C had stepped surface near the edges of particles (Fig. 4c). It was obvious that as calcination temperature increases, the nanocrystal would grow and the pore collapsed.

Fig. 5 (a) and (b) shows the TEM image of the Pt- and Au-loaded m-Nb_2O_5 catalysts, respectively. During the photodeposition procedure, the Pt particles deposited appear as small black spots, showing uniformly dispersed Pt nanoparticles on the framework of mesoporous Nb_2O_5. Based on TEM image analysis, the average particle size of Pt was 2.2 nm. This suggested that the migration barriers of the Pt species on mesoporous Nb_2O_5 catalyst was high and hindered the growth of the large Pt particle. This behavior allowed us to synthesize ultra fine Pt particles on mesoporous Nb_2O_5. Furthermore, the gold particles of Au/m-Nb_2O_5 catalyst confirm the appearance of gold agglomeration. As shown in Fig. 5(b) the particle distribution of Au, revealing that the particles are 25–60 nm in size, and the average particle size of Au was 32 nm. The results were similar to those previously reported for supported Au nanoparticles prepared by photo deposition method [16,17]. In contrast to Pt- and Au-loaded m-Nb_2O_5 catalysts, no Cu particles can be observed in the TEM image of Cu/m-Nb_2O_5 (Fig. 5(c)) and we can hardly find NiO nanoparticle on NiO/m-Nb_2O_5 (Fig. 5(d)), indicating that nickel and copper species should be highly dispersed within the mesoporous sturcture of Nb_2O_5.

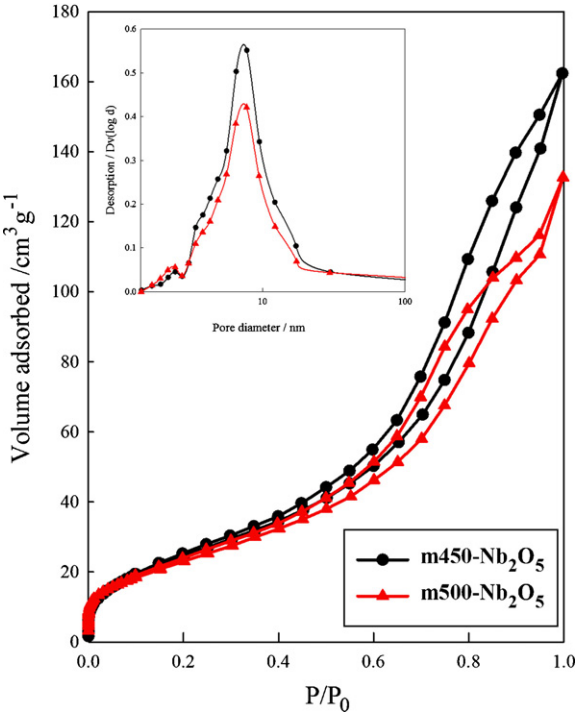

Fig. 6. N_2 adsorption hysteresis loops and BJH pore size distribution: (a) m450-Nb_2O_5 and (b) m500-Nb_2O_5.

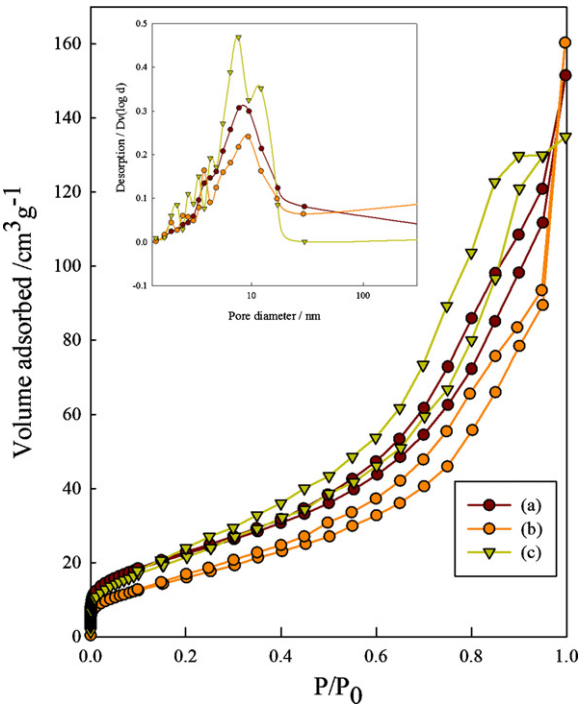

Fig. 7. N_2 adsorption hysteresis loops and BJH pore size distribution: (a) Pt/m450-Nb_2O_5, (b) Cu/m-Nb_2O_5 and (c) NiO/m-Nb_2O_5.

Fig. 6 shows the N_2 adsorption–desorption isotherms of m450-Nb_2O_5, and m500-Nb_2O_5 as well as the pore size distribution curves. The physical characterization of these samples is also shown in Table 1. As seen in Fig. 6, the N_2 adsorption–desorption isotherms of the two samples exhibit typical type IV of IUPAC classification. The steep increase in N_2 adsorption with increasing relative pressure, P/P_0, and the amount of N_2 adsorbed reaching ca. 18 cm^3/g at $P/P_0 = 0.1$ suggest the presence of an appreciable amount of micropores on the m450-Nb_2O_5 surfaces. The mild increase in N_2 adsorption ranging from $P/P_0 = 0.1$ to 0.95 reveals the presence of mesopores. The hysteresis loop with such a contour ranging from $P/P_0 = 0.5$ to 0.95 is related to the surface pores of an almost cylindrical shape. Compared with the m450-Nb_2O_5 sample, the m500-Nb_2O_5 sample seems to possess plenty of almost cylindrical pores yet with larger pore size owing to the slight shift of the loop toward higher relative pressure. The surface area of m500-Nb_2O_5 sample decreased slightly (form 108 to 89 m^2/g), certifying that the pore structure was damaged. As clearly shown in Table 1, the surface area of the m650-Nb_2O_5 sample was 31 m^2/g, which is smaller than those of m450-Nb_2O_5 or m500-Nb_2O_5 indicating the collapse of the mesoporous structure.

Fig. 7 shows the N_2 adsorption–desorption isotherms of Pt/m-Nb_2O_5, Cu/m-Nb_2O_5, and NiO/m-Nb_2O_5 samples as well as the pore size distribution curves. The texture properties of these metal loaded mesoporous Nb_2O_5 samples are summarized in Table 1. It is seen that the surface areas of NiO/m-Nb_2O_5, and Pt/m-Nb_2O_5 and Au/m-Nb_2O_5 were decreased slightly after loading cocatalyst and had a larger pore size than m450-Nb_2O_5. It evidenced that the mesoporous structure of Nb_2O_5 was well retained after loading cocatalysts. However, the surface area of Cu/m-Nb_2O_5 decreased to 64 m^2/g which was attributed the increasing crystallite growth of Nb_2O_5 during the reduction treatment of Cu at 500 °C which was conformed to the XRD studies.

The light absorption capacity of photocatalysts influences the efficiency of any photocatalytic reaction. Fig. 8 shows the UV–vis diffuse reflectance spectra of the mesoporous Nb_2O_5 samples prepared by different thermal treatments. As can be seen, both m-Nb_2O_5 and m500-Nb_2O_5 had an absorption edge at around 367 nm. The m650-Nb_2O_5 shifted to the long-wavelength region at high calcination temperature, showing an absorption edge at about 420 nm. The bandgap can be estimated by extrapolating the rising portion of the UV spectrum to the abscissa at zero absorption [18]. The estimated bandgap of m450-Nb_2O_5, m500-Nb_2O_5 and m650-Nb_2O_5 are 3.17, 3.09 and 2.99 eV, respectively. The band gap of mesoporous Nb_2O_5 was clearly decreased with increasing calcination temperature. Such difference might be due to the variations in crys-

Table 1
Physical properties and photocatalytic H_2 evolution rates on mesoporous Nb_2O_5 and cocatalyst loaded mesoporous Nb_2O_5 catalysts.

Catalyst	Surface area (m^2/g)	Average pore size (nm)	H_2 production ($\mu mol\ h^{-1}\ g^{-1}$)
m450-Nb_2O_5	108	7.6	328
m500-Nb_2O_5	89	7.8	259
m650-Nb_2O_5	31	–	245
Au/m-Nb_2O_5	100	9.5	2091
Pt/m-Nb_2O_5	84	8.5	4647
Cu/m-Nb_2O_5	64	9.3	1572
NiO/m-Nb_2O_5	92	10	709
C-Nb_2O_5	–	–	8.5
TiO_2 (Degussa P25)	–	–	100.7

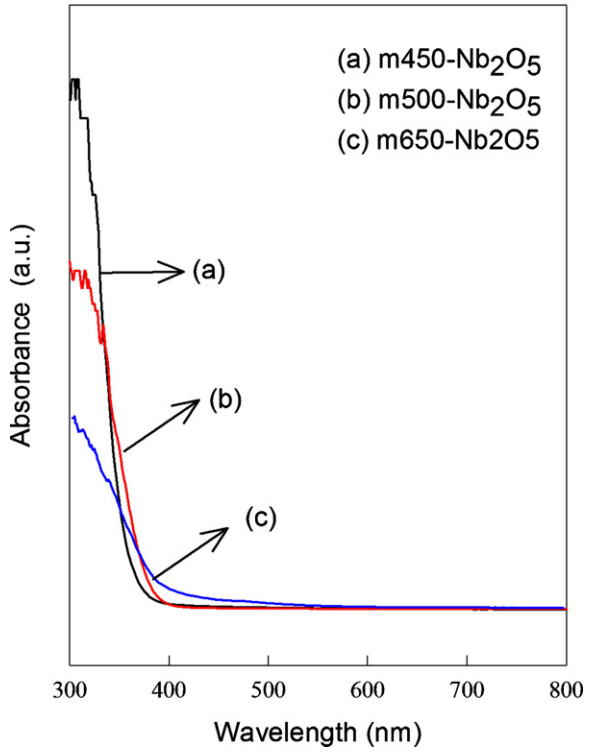

Fig. 8. UV–vis spectra of (a) m450-Nb_2O_5, (b) m500-Nb_2O_5 and (c) m650-Nb_2O_5.

tal size of photocatalysts. Similar results were reported by Chen et al. [15], where the smaller crystal size of Nb_2O_5 trended to have a blue shift of optical absorption or larger energy band gap, possibly caused by quantum-size effect [19].

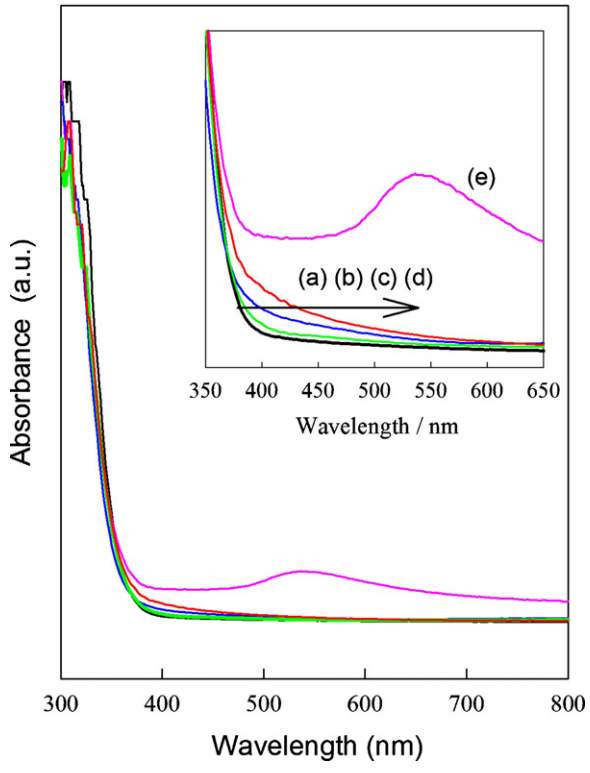

Fig. 9. UV–vis spectra of (a) m450-Nb_2O_5, (b) NiO/m-Nb_2O_5, (c) Cu/m-Nb_2O_5, (d) Pt/m-Nb_2O_5 and (e) Au/m-Nb_2O_5.

Fig. 9 shows the UV–vis spectra that show the influence of co-catalysts (Au, Pt, Cu and NiO) on UV–vis absorption. In this study, all the metal loading of catalysts was maintained at about 1 wt% in order to investigate the effects of other variables. As can be seen, the absorption edge of m-Nb_2O_5 can be engineered toward longer wavelength by introduction of Au, Pt, Cu and NiO. This is attributed the metal clusters give rise to localized energy levels of mesoporous Nb_2O_5. In this work, the change in red shift was of the following order: m-Nb_2O_5 < NiO/m-Nb_2O_5 < Cu/m-Nb_2O_5 < Pt/m-Nb_2O_5 < Au/m-Nb_2O_5. Previous work [11] demonstrated that large NiO_x cocatalyst particles (~30 nm) was formed on $K_4Nb_6O_{17}$ surface during incipient wetness impregnation process, whose UV–vis spectra showed a broad absorption shoulder in the visible light region. This result is similar to that of Cu/TiO_2 [20]. Note in Fig. 9(a–c), the UV–vis spectra of NiO- and Cu-loaded m450-Nb_2O_5 employed in this work were similar to bare m450-Nb_2O_5, the modification only slightly increased the optical absorption in 400 nm–550 nm, indicating that the NiO and Cu cocatalyst particles on m450-Nb_2O_5 should be quite small.

Furthermore, the absorption edge of Pt/m-Nb_2O_5 shifted to longer wavelength and a small absorption shoulder appeared in the visible light region (Fig. 4 d). This is because the Pt clusters give rise to localized energy levels in the band gap of m-Nb_2O_5. In Fig. 9(e), the absorption edge of Au/m-Nb_2O_5 is further shifted to the visible side, and showed a strong surface plasma resonance absorption peak of gold particles in response to optical excitation of Au nanoparticles at 560 nm [17]. Furthermore, a shoulder peak at around 530 nm was observed, this absorption is due to collective oscillation of free conduction band electrons of gold particles in response to optical excitation [21]. The estimated bandgap of m450-Nb_2O_5, 1wt%NiO/m-Nb_2O_5 and 1wt%Cu/m-Nb_2O_5 are almost identical. On the other hand, Pt/m-Nb_2O_5 and Au/m-Nb_2O_5 causes a slight band gap narrowing which were 3.03 eV and 2.99 eV, respectively.

3.2. *Photocatalytic water splitting on the mesoporous Nb_2O_5 and cocatalyst loaded mesoporous Nb_2O_5 catalysts*

Fig. 10 displays the effect of calcination condition on the water splitting ability of niobium oxide for hydrogen production. Commercial Nb_2O_5 (C-Nb_2O_5) and TiO_2 (Degussa P25) was used for comparison. The H_2 production stopped when light was turned off (dark region) and similar hydrogen productions were observed in the three repeat runs indicated that the water splitting of aqueous methanol solution on these catalysts was photocatalytic. This indicates that the water splitting in aqueous methanol solution on these catalysts was photocatalytic and that the catalysts can be used repeatedly without deactivation. Although methanol acted as an efficient hole scavenger and inhibited the charge recombination during the water splitting reaction [22], only trace amount of CO_2 was observed by the non-dispersive infrared (NDIR) CO_2 sensor. This is probably due to the fact that conversion of methanol-derived adsorbate into CO_2 by photo-excited holes is a slow process in the oxidation of methanol [23]. The average production rate of hydrogen from water splitting over this period are listed in Table 1 which increased as the following order: C-Nb_2O_5 < TiO_2 (Degussa P25) < m650-Nb_2O_5 < m500-Nb_2O_5 < m450-Nb_2O_5. Commercial Nb_2O_5 catalyst exhibited lowest activity which was slightly lower than commercial TiO_2 (Degussa P25). The activity of mesoporous Nb_2O_5 mixed oxides catalysts drastically increased at least 28 times as compared to commercial Nb_2O_5, and also exhibited a much higher photocatalytic activity than that of TiO_2 (P25). The m450-Nb_2O_5 catalyst which has largest surface area, offers a higher number of active sites by unit mass thus lead to a higher photocatalytic activity.

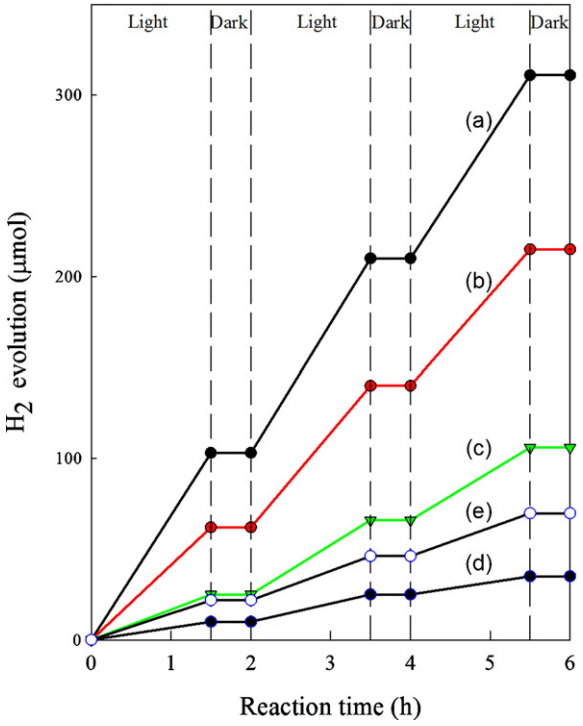

Fig. 10. Time course of H_2 evolution (a) m450-Nb_2O_5, (b) m500-Nb_2O_5, (c) m650-Nb_2O_5, (d) c-Nb_2O_5 and (e) TiO_2 (Degussa P25).

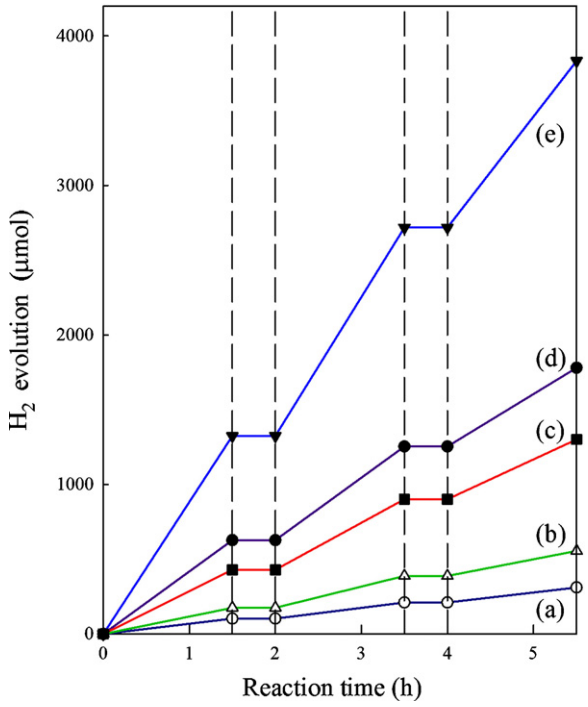

Fig. 11. Time course of H_2 evolution: (a) m450-Nb_2O_5, (b) NiO/m-Nb_2O_5, (c) Cu/m-Nb_2O_5, (d) Au/m-Nb_2O_5 and (e) Pt/m-Nb_2O_5.

It is known that surface area and crystallinity are two key factors of the photocatalytic activity of photocatalyst. Photocatalyst with a high specific surface area offers a higher number of active sites and photocatalyst with high crystallinity have low concentration of defects which act as recombination centers of photo-exited carriers. However, the surface area and crystallinity are always the competition factors. Yu et al. [24] reported that increasing hydrothermal time of synthesis of mesoporous TiO_2 increased crystallite size of mesoporous TiO_2 thus enhanced the photocatalytic activity of acetone oxidation. However, BET specific surface area and porosity steadily decreased with increasing hydrothermal time, which led to a decrease in photocatalytic activity. Jitputti et al. [25] reported that mesoporous TiO_2 calcined at 550 °C with a higher crystallinity of the anatase phase showed a higher H_2 production per S_{BET} of photocatalyst ($\mu mol\,m^{-2}$) than mesoporous TiO_2 calcined at 500 °C. However, mesoporous TiO_2 calcined at 500 °C with a lager surface area gave at higher amount of H_2 production based on weight of photocatalyst. Our results are similar to those observed on mesoporous TiO_2. As cacinated at higher temperature, the surface area of mesoporous Nb_2O_5 was decreased and the crystal size of niobium oxide was increased. Furthermore, though m650-Nb_2O_5 catalyst showed a lower hydrogen production rate (245 $\mu mol\,h^{-1}\,g^{-1}$) than m450-Nb_2O_5 (328 $\mu mol\,h^{-1}\,g^{-1}$), it exhibited a higher specific photocatalytic activity (8 $\mu mol\,h^{-1}\,m^2$) than m450-Nb_2O_5 (3 $\mu mol\,h^{-1}\,m^2$).

Fig. 11 shows the H_2 evolution significantly changed with the variation of metal (Pt, Au, Cu and NiO) loaded on m-Nb_2O_5. As expected, the H_2 production rate significantly enhanced after loading cocatalyst. Shown clearly in the Table 1, the formation rates of H_2 increased as the following order: m450-Nb_2O_5 < NiO/m-Nb_2O_5 < Cu/m-Nb_2O_5 < Au/m-Nb_2O_5 < Pt/m-Nb_2O_5. The most active photocatalyst was Pt/m-Nb_2O_5. The magnitude of this photocatalytic activity is more than 14 times of that of m450-Nb_2O_5 alone. Mesoporous Nb_2O_5 with noble metal cocatalyst (Pt and Au) showed a much higher activity than NiO and Cu loaded mesoporous Nb_2O_5 photocatalyst. These can attributed that noble metal nanoparticles are considered to be highly electronegative as their Fermi level can be shifted to negative potentials owing to charge accumulating effects [26], that significantly enhances the photocatalytic efficiency for water splitting reaction. The reason for the highest activity of Pt/m-Nb_2O_5 could be the small Pt particle size. Well dispersed Pt clusters into the mesoporous niobium oxide texture, average crystallite size is 2.2 nm which acted as sink for photo induced charge carriers, promotes interfacial charge transfer process. It should be noticed that due to the high price and limited availability of noble metal resources, Cu is a cheap and widely available candidate for high performance cocatalyst. The formation rate of H_2 on Cu/m-Nb_2O_5 is about 185 and 16 times than Bulk-Nb_2O_5 and TiO_2 (P25) catalyst.

4. Conclusions

A series mesoporous Nb_2O_5 with Pt, Au, Cu and NiO cocatalyst were synthesized successfully. The influence of various calcination conditions on mesoporous Nb_2O_5 also was discussed. Our experimental reveals mesoporous Nb_2O_5 calcined at 450 °C formed wormlike mesoporous structure composed by nanocrystallization Nb_2O_5 and had a high surface area, leading to a high photocatalytic activity. Calcination temperatures exhibited a strong influence on the structure and crystallinity of mesoporous Nb_2O_5. Mesoporous Nb_2O_5 calcined at 650 °C showed a higher specific photocatalytic activity than the 450 °C calcined sample due to better Nb_2O_5 crystallinity. However, the photocatalytic activity of m650-Nb_2O_5 was lower than m450-Nb_2O_5 which can be attributed to the low surface area originating from the high temperature calcination.

The rate of H_2 evolution from an aqueous methanol solution under UV irradiation significantly changed with the variation of loading metal. The photoactivity of water splitting over mesoporous Nb_2O_5 with Pt, Au, Cu and NiO cocatalyst increased as the following order: m450-Nb_2O_5 < NiO/m-Nb_2O_5 < Cu/m-Nb_2O_5 < Au/m-Nb_2O_5 < Pt/m-Nb_2O_5.

The Pt/m-Nb_2O_5 showed an ultra high photocatalytic activity with a rate of H_2 production of 4647 $\mu mol\,h^{-1}\,g^{-1}$, which was about

2.2, 2.9 and 6.5 times than Au, Cu and NiO photocatalysts, respectively. This was attributed to the well dispersed Pt nanoparticles cased an efficient electron–hole separation in the photocatalyst.

Acknowledgement

The authors thanks the financial support from NSC Taiwan under the grant of NSC 98-2221-E-259-012-MY2.

References

[1] A. Fujishima, K. Honda, Nature 238 (1972) 37–38.
[2] K. Sayama, K. Mukasa, R. Abe, Y. Abe, H. Arakawa, J. Photochem. Photobiol. A 148 (2002) 71–77.
[3] T. Takata, Y. Furumi, K. Shinohara, A. Tanaka, M. Hara, J.N. Kondo, K. Domen, Chem. Mater. 9 (1997) 1063–1064.
[4] D.W. Hwang, H.G. Kim, J. Kim, K.Y. Cha, Y.G. Kim, J.S. Lee, J. Catal. 193 (2000) 40–48.
[5] J. Sato, N. Saito, H. Nishiyama, Y. Inoue, J. Photochem. Photobiol. A 148 (2002) 85.
[6] Z.B. Lei, G.J. Ma, M.Y. Liu, W.S. You, H.J. Yan, G.P. Wu, T. Takata, M. Hara, K. Domen, C. Li, J. Catal. 237 (2006) 322.
[7] M.K. Tian, W.F. Shangguan, J. Yuan, L. Jiang, M.X. Chen, J.W. Shi, Z.Y. Ouyang, S.J. Wang, Appl. Catal. A 309 (2006) 76–84.
[8] A. Ishikawa, T. Takata, J.N. Kondo, M. Hara, H. Kobayashi, K. Domen, J. Am. Chem. Soc. 124 (2002) 13547–13553.
[9] D. Wang, Z. Zou, J. Ye, Chem. Phys. Lett. 373 (2003) 191–196.
[10] H. Kato, K. Asakura, A. Kudo, J. Am. Chem. Soc. 125 (2003) 3082–3089.
[11] H.Y. Lin, T.H. Lee, C.Y. Sie, Int. J. Hydrogen Energy 33 (2008) 4055–4063.
[12] H.Y. Lin, H.C. Huang, W.L. Wang, Micropor. Mesopor. Mater. 115 (2008) 568–575.
[13] P. Yang, D. Zhao, D.I. Margolese, B.F. Chmelka, G.D. Stucky, Nature 396 (1998) 152–155.
[14] B. Lee, T. Yamashita, D.L. Lu, J.N. Kondo, K. Domen, Chem. Mater. 14 (2002) 867.
[15] X.Y. Chen, T. Yu, X.X. Fan, H.T. Zhang, Z.S. Li, J.H. Ye, Z.G. Zou, Appl. Surf. Sci. 253 (2007) 8500.
[16] H.-Y. Lin, Y.-S. Chang, Int. J. Hydrogen Energy 35 (2010) 8463–8471.
[17] A. Iwase, H. Kato, A. Kudo, Catal. Lett. 108 (2006) 6–10.
[18] E. Sanchez, T. Lopez, Mater. Lett. 25 (1995) 271–275.
[19] R. Brayner, F. Bozon-Verduraz, Phys. Chem. Chem. Phys. 5 (2003) 1457.
[20] H.C. Yang, H.Y. Lin, Y.S. Chien, J.C.S. Wu, H.H. Wu, Catal. Lett. 131 (2009) 381–387.
[21] R.S. Sonawane, M.K. Dongare, J. Mol. Catal. A: Chem. 243 (2006) 68.
[22] A. Yamakata, T.A. Ishibashi, J. Onishi, J. Phys. Chem. B 107 (2003) 9820–9823.
[23] Z. Yu, S.S.C. Chuang, J. Catal. 246 (2007) 118–126.
[24] J. Yu, G. Wang, B. Cheng, M. Zhou, Appl. Catal. B-Environ. 69 (2007) 171–180.
[25] J. Jitputti, S. Pavasupree, Y. Suzuki, S. Yoshikawa, J. Solid State Chem. 180 (2007) 1743.
[26] A.L. Linsebigler, G. Lu, T. John, Yates Jr., Chem. Rev. 95 (1995) 735–758.